Solar Phys
DOI 10.1007/s11207-013-0303-y

Multiwavelength Observations of an Eruptive Flare: Evidence for Blast Waves and Break-Out

Pankaj Kumar · D.E. Innes

Received: 6 June 2012 / Accepted: 5 April 2013

Abstract Images of an east-limb flare on 3 November 2010 taken in the 131 Å channel of the *Atmospheric Imaging Assembly* onboard the *Solar Dynamics Observatory* provide a convincing example of a long current sheet below an erupting plasmoid, as predicted by the standard magnetic reconnection model of eruptive flares. However, the 171 Å and 193 Å channel images hint at an alternative scenario. These images reveal that large-scale waves with velocity greater than 1000 km s^{-1} propagated alongside and ahead of the erupting plasmoid. Just south of the plasmoid, the waves coincided with type-II radio emission, and to the north, where the waves propagated along plume-like structures, there was increased decimetric emission. Initially, the cavity around the hot plasmoid expanded. Later, when the erupting plasmoid reached the height of an overlying arcade system, the plasmoid structure changed, and the lower parts of the cavity collapsed inwards. Hot loops appeared alongside and below the erupting plasmoid. We consider a scenario in which the fast waves and the type-II emission were a consequence of a flare blast wave, and the cavity collapse and the hot loops resulted from the break-out of the flux rope through an overlying coronal arcade.

Keywords Coronal loops · Flux rope · Magnetic field · Magnetic reconnection · Solar flares

Electronic supplementary material The online version of this article (doi:10.1007/s11207-013-0303-y) contains supplementary material, which is available to authorized users.

P. Kumar (✉)
Korea Astronomy and Space Science Institute (KASI), Daejeon, 305-348, Republic of Korea
e-mail: pankaj@kasi.re.kr

P. Kumar · D.E. Innes
Max-Planck Institut für Sonnensystemforschung, 37191 Katlenburg-Lindau, Germany

D.E. Innes
e-mail: innes@mps.mpg.de

Published online: 25 April 2013

1. Introduction

The flare and flux rope eruption observed on the east limb of the Sun on 3 November 2010 showed many of the expected features of eruptive flare models (Carmichael, 1964; Sturrock, 1966; Hirayama, 1985; Kopp and Pneuman, 1976). In particular, a fast moving plasmoid, interpreted as a flux rope, appeared above the flare site with what looked like a long, hot current sheet below (Reeves and Golub, 2011; Cheng *et al.*, 2011; Savage *et al.*, 2012; Hannah and Kontar, 2012). Hot, inflowing plasma was observed below the plasmoid, seemingly causing it to accelerate and drive a shock, indicated by type-II radio emission, in the low corona (Bain *et al.*, 2012; Zimovets *et al.*, 2012). The eruption also triggered transverse oscillations in the surrounding loop systems (White and Verwichte, 2012; White, Verwichte, and Foullon, 2012).

To understand the connection between the loops and the erupting plasmoid, we carefully investigated the relation between the hot (131 Å) and cooler (193 and 171 Å) plasma emission. This revealed fast waves along plumes outside the hot cavity that were also headed by enhanced radio emission, suggesting that the flare caused shock-like signatures considerably beyond the plasmoid, possibly due to a flare blast wave. Although blast waves at the onset of energetic flares are predicted (Vršnak and Lulić, 2000a, 2000b; Vršnak and Cliver, 2008; Magdalenić *et al.*, 2008, 2010), they have proved difficult to observe. One major problem was that they propagate with speeds greater than 1000 $\mathrm{km\,s^{-1}}$, and therefore required high image cadence and a large field of view to be detected in images. Thus it was not until images from the *Atmospheric Imaging Assembly* (AIA; Lemen *et al.*, 2012) became available that there was a reasonable chance of seeing them. Blast waves have been invoked, however, to explain the high (greater than 500 $\mathrm{km\,s^{-1}}$) Doppler shifts observed in Fe XIX and Fe XX ultraviolet emission lines seen across a significant fraction of flaring active region coronae (Innes *et al.*, 2001; Tothova, Innes, and Stenborg, 2011), and also in events exhibiting type-II radio bursts where there was only slow or no associated coronal mass ejection (CME) (Vršnak *et al.*, 2006; Magdalenić *et al.*, 2012).

The 3 November 2010 eruption is also significant because of its well-observed inflows below the erupting plasmoid, which have been interpreted as inflows to a current sheet. As pointed out by Hannah and Kontar (2012), these inflows are hot (8 – 14 MK), not cool, as predicted by the standard model. If the fast waves result from a flare blast wave, then the plasmoid acceleration may have occurred before the inflows, and this leads us to consider the possibility that the inflows are a consequence of flux rope break-out through the overlying coronal arcade (Antiochos, DeVore, and Klimchuk, 1999; Karpen, Antiochos, and DeVore, 2012). Break-out leads to reconnection in the corona, the outward acceleration of the flux rope, and the formation of post-flare loops on the side and below the break-out site, as well as inflows to a current sheet below the flux rope. We therefore investigate in more detail the structure of the flare-heated plasma seen in the 131 and 94 Å images to understand the dynamics beyond the regions of the previously identified inflows and current sheet.

In this paper we first show the evidence for fast propagating waves and their relation to enhanced radio emission. We then compare the timing of the break-out with the onset of plasma inflow below the plasmoid, and the structures seen in the 131 and 94 Å channel emissions. A summary sketch of the observed structures and our interpretation is given in the final section.

2. Observations and Results

The eruption occurred in active region NOAA 11121, which appeared on the eastern limb (N38E18) on 3 November 2010. The C4.9 flare was first seen in STEREO-B *Extreme Ultra-Violet Imager* (EUVI; Howard *et al.*, 2008) images at 12:10 UT and had a hard X-ray onset at 12:13 UT and peak at 12:14 UT (Zimovets *et al.*, 2012). The event, observed by the AIA on-board the *Solar Dynamics Observatory* (SDO; Pesnell, Thompson, and Chamberlin, 2012), the *Reuven Ramaty High Energy Solar Spectroscopic Imager* (RHESSI; Lin *et al.*, 2002), the *Nançay Radioheliograph* (NRH; Kerdraon and Delouis, 1997), and the San Vito Radio Solar Telescope has caught attention because several of its features resemble the standard flare model and has presented a plausible case for a piston-driven shock (Bain *et al.*, 2012; Zimovets *et al.*, 2012).

In this analysis, we discuss AIA 131, 94, 193, and 171 Å image sequences taken with a cadence of 12 s. Most of the images are shown after the subtraction of a pre-flare image taken at approximately 12:10 UT (*i.e.*, base-difference images) to reveal the changes caused by the flare. To find the location of the radio emission, we used high-cadence radio images of the Sun from the NRH, which operates in the frequency range of 160 – 435 MHz and probes the coronal plasma at heights $\leq 1.5\ R_{\odot}$ (Kerdraon and Delouis, 1997).

An overview of several of the features discussed in previous papers is shown in Figure 1. The 131 Å image, dominated by Fe XXI emission, shows a hot, $\approx$10 MK, plasmoid directly above and connected to the flare site by a long, thin thread, which has been interpreted as a current sheet (CS). The plasmoid swept up the surrounding plasma into a bright rim of cooler, $\approx$2 MK, 193 Å emitting plasma (Reeves and Golub, 2011; Cheng *et al.*, 2011). Radio observations revealed a type-II radio burst near the leading edge of the expanding plasmoid system (Bain *et al.*, 2012; Zimovets *et al.*, 2012). Behind the plasmoid were hot plasma inflows (Savage *et al.*, 2012) that converged toward CS. The ripples along the northern flank of the hot cavity have been interpreted as Kelvin–Helmholtz (KH) roll-ups (Foullon *et al.*, 2011). Important features that we discuss below are also illustrated in the 193 Å (Figure 1b) and 171 Å (Figure 1c) base-difference images. Here dark represents pre-flare active region structures that have disappeared due to heating or eruption. For example, the dark loop in the 193 Å image corresponds to a pre-flare coronal loop or arcade. The 171 Å base-difference image shows that there was enhanced emission both south and north of the hot plasmoid cavity.

2.1. Early EUV Waves

During the early stage of the flare/flux-rope eruption, fast waves were observed in sequences of 171 Å images. Figure 2 is a composite of AIA 171 Å and 131 Å base-difference images showing the regions and directions of the fast waves. This is one frame from the movie linked to the figure in the online version. In Figure 2, the extreme ultraviolet (EUV) wave south of the plasmoid is visible as enhanced 171 Å emission extending beyond the height of the 131 Å plasmoid. The enhanced emission seen in the north at this time is probably caused by resonance scattering of EUV flare emission because the whole region brightened simultaneously and propagating waves were not seen here until 12:15:00 UT. The wave speeds can be deduced from the space–time images shown in Figure 3. This method computes the time of an abrupt change in the intensity at each spatial position. Then a linear function is fitted to the values to obtain the velocity. When the front changes speed, it is sensitive to the start and end distance used to fit the wave front. For example, the front in Figure 3b changed from 1200 $\mathrm{km\,s^{-1}}$ at the start to 700 $\mathrm{km\,s^{-1}}$ at the end. In the image, we plot a line corresponding to the best estimate of the velocity and provide the velocity range. The

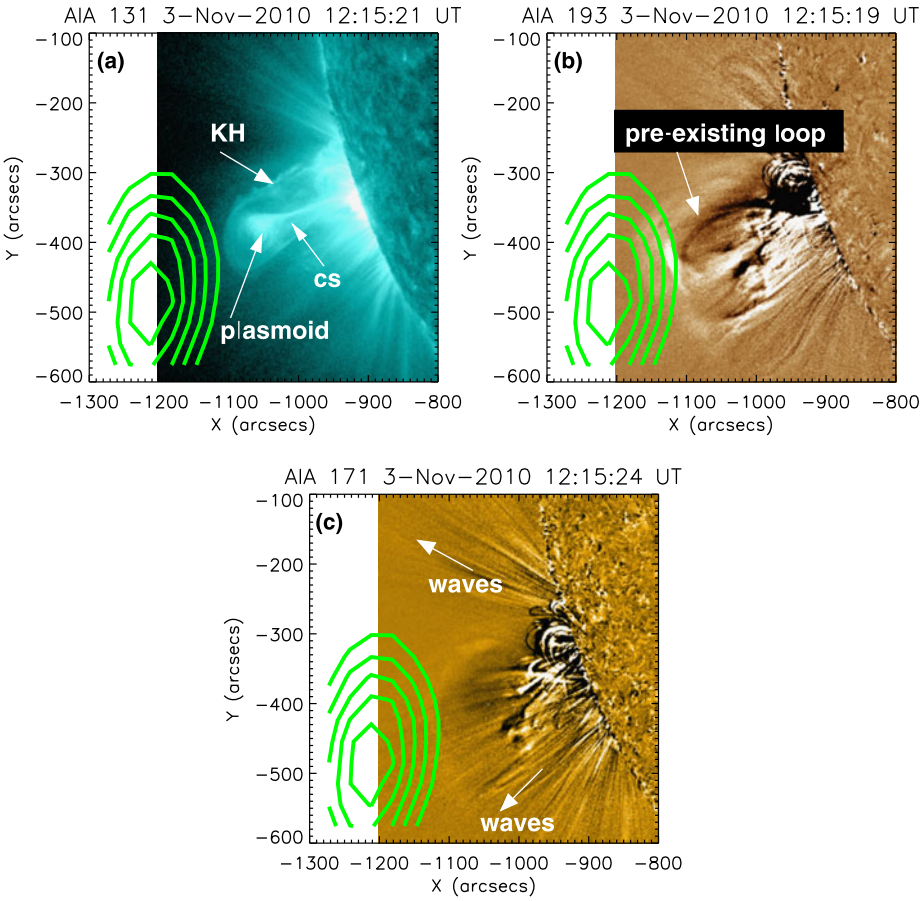

Figure 1 SDO/AIA images of the 3 November 2010 eruption with radio 270 MHz contours at 50 %, 60 %, 70 %, 80 %, and 90 % of maximum. (a) 131 Å intensity with previously identified current sheet (CS), plasmoid, and Kelvin–Helmholtz roll-ups (KH) marked. (b) 193 Å base difference showing the position of the pre-existing loop as a dark loop. (c) 171 Å base difference. The 171 Å and 131 Å base images were taken at 12:09:00 and 12:09:09 UT, respectively.

waves to the south had a very high plane-of-sky speed, about 2200 km s^{-1}. The speed was about twice that of the plasmoid and the waves along the plumes to the north. The southern waves and the plasmoid eruption started at 12:13 UT, several minutes before the waves to the north. The composite AIA 131 and 171 Å base-difference movie clearly shows the bright EUV wavefront south of the 131 Å plasmoid, and the propagation of the EUV wave along the plumes, north of the flare site.

2.2. Radio Emission

The radio emission has been discussed in the context of the RHESSI hard X-ray emission in Zimovets *et al.* (2012) and Bain *et al.* (2012). At flare onset there was a short burst of hard X-ray (25 – 50 keV) and microwave (3000 – 5000 MHz) emission, peaking at ≈ 12:14 UT. A few minutes later, there was a decimetric type-II radio burst that showed distinct band-splitting, indicating two outward-moving sources. Zimovets *et al.* (2012) interpreted these

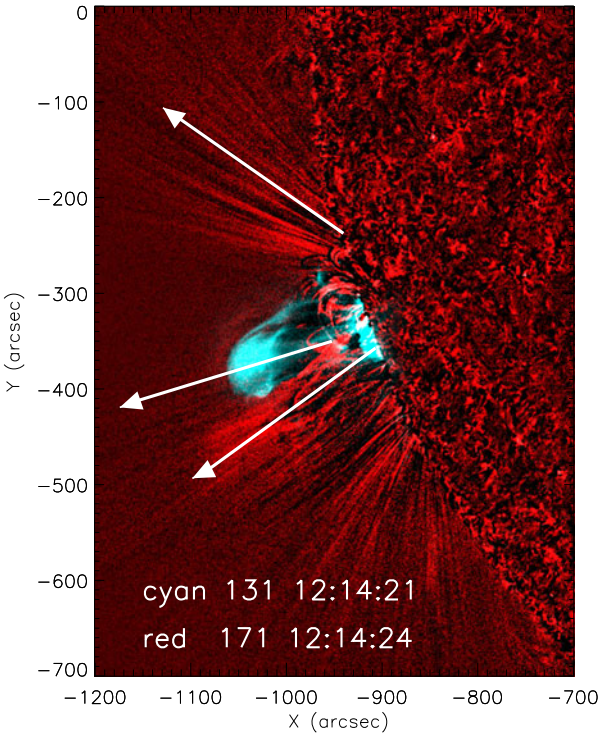

Figure 2 Composite of 131 Å (cyan) and 171 Å (red) base-difference images showing a broad enhanced front of 171 Å emission just south of the hot plasmoid, observed at 131 Å. The white lines show the position of the space–time images in Figure 3. This is one frame from the movie *131_171.avi*.

as the up- and downstream regions of a shock but it is also possible that the splitting is caused by waves along two different density structures. Zimovets *et al.* (2012) found that one source started slightly off-set (100 Mm) to the south of the hot plasmoid trajectory, and had a speed 2240 km s^{-1}, whereas the other was in line with the plasmoid and had a velocity of 1500 km s^{-1}.

In Figure 4, we compare the timing and sites of the radio emission with the waves. Figure 4a shows that early on there was enhanced 445 and 432 MHz emission across a large portion of the active region, with the most intense emission on either side of the erupting plasmoid. The southern radio source is the low-frequency component tracked in Zimovets *et al.* (2012) and estimated to have a velocity 2240 km s^{-1}. As can be seen in the images, it coincided with the trajectory of the fast 2200 km s^{-1} waves inferred from the 171 Å images, so it is possible that the waves excited this component of the radio emission.

The second component, which was labeled high-frequency component in Zimovets *et al.* (2012), was seen along the trajectory of the hot plasmoid. It did not appear until 1 min later at 327 MHz (Figure 4b), and had a speed of 1500 km s^{-1}, which was faster than the hot plasmoid plane-of-sky speed, and close to the speed of the 211 Å leading edge (Zimovets *et al.*, 2012). Subsequently, emission in front of the plasmoid dominated at frequencies at and below 327 MHz, and both high- and low-frequency radio components appeared across an extended region above the plasmoid. The radio emission may then have been produced by up- and downstream regions of a shock or by waves along different structures, as suggested in earlier images.

In Figure 4, we also show 150 MHz contours. This emission comes from waves in lower density plasma than the higher frequency emission, so it is seen later and higher in the corona when caused by an outward-propagating source. On this day, there was a 150 MHz

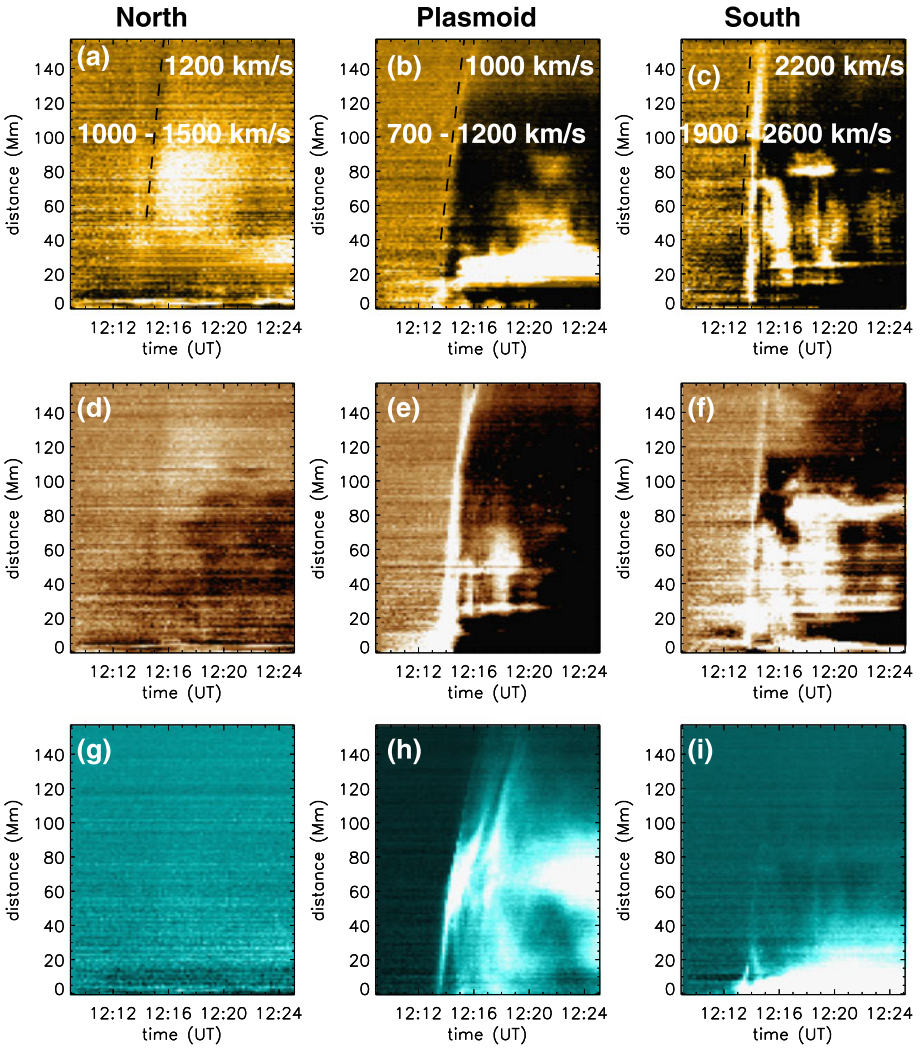

Figure 3 Space-time base-difference images of 171 Å (top row), 193 Å (middle), and 131 Å (bottom) emission along the three white lines shown in Figure 2. The left column is along the northern line, the middle along the plasmoid, and the right column along the southern line. Dashed black lines show the track for a front with the labeled speed.

frequency source at the head of the northern plumes (Figure 4a) where the northern 171 Å fast waves were observed. This source had been there long before the flare and it brightened at the time of the flare (Figure 4f). The NRH maps at the time of the early 150 MHz source brightening are shown in Figure 4b. The center of the 150 MHz emission moved in front of the hot plasmoid at 12:16:24 UT as part of the type-II burst. Later, as the flare evolved, the centroid of the low-frequency (150 – 327 MHz) emission moved south (Figures 4d and 4e). The location of the radio sources with respect to the eruption site is shown in Figure 4e, where we have overlaid radio source (150, 228, and 327 MHz) contours on the AIA 193 Å running-difference image of the eruption at 12:15:19 UT. This image shows that from

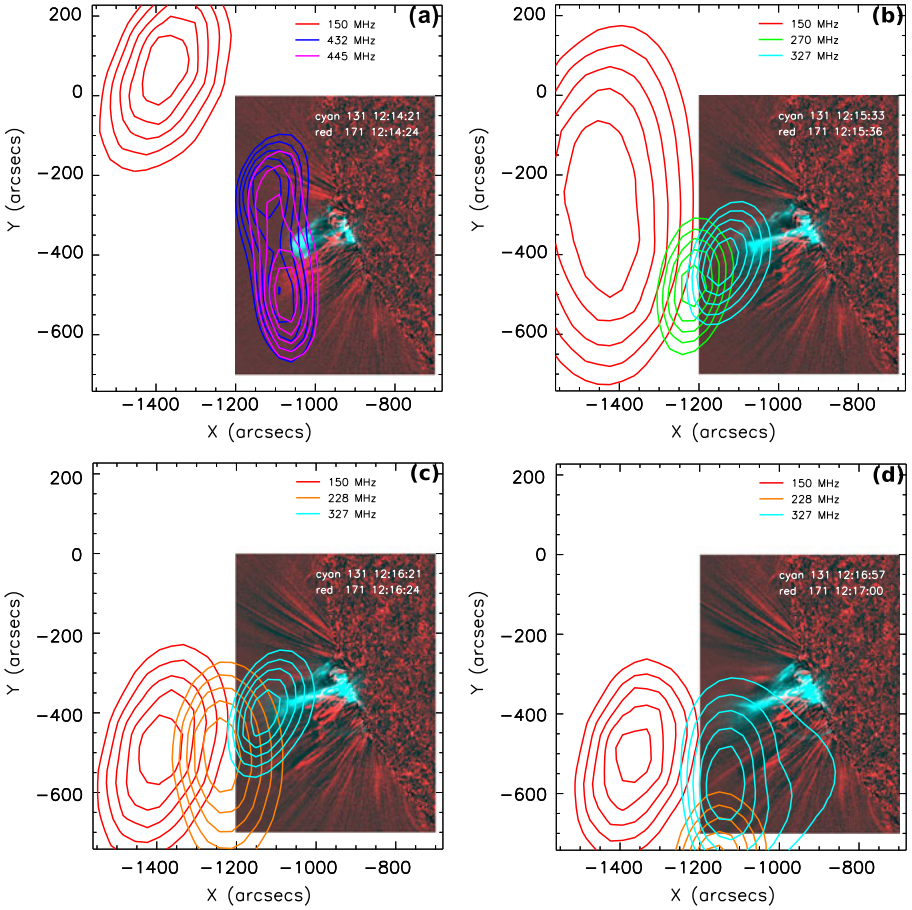

Figure 4 Evolution of radio emission in the context of the EUV waves and hot plasmoid. The bottom panels show the drifting type-II sources indicated by arrows.

12:14 – 12:19 UT, the radio sources drifted southward (indicated by an arrow). Figure 4f displays the integrated radio flux profiles (in sfu) at four frequencies obtained from NRH. It is interesting to see the drifting type-II source (indicated by red arrows) at all frequencies.

2.3. Break-Out

Break-out occurred when the flux-rope broke through the overlying cavity system. Several structural changes appeared at the time of break-out. The overlying loop system disrupted and the plasmoid structure changed. At the same time, a hot thread of emission appeared below and attached to the plasmoid, and the earlier expansion of the cavity changed to contraction.

Some of these features are illustrated in Figure 5. These are time-distance images taken across (top) and along (bottom) the direction of propagation of the erupting flux rope, as shown in Figure 6b. These two perpendicular directions were chosen because they allow one to compare the expanding and contracting cavity below the plasmoid and the outward-propagating waves. The first dashed line marks the flare onset time, and the second dashed

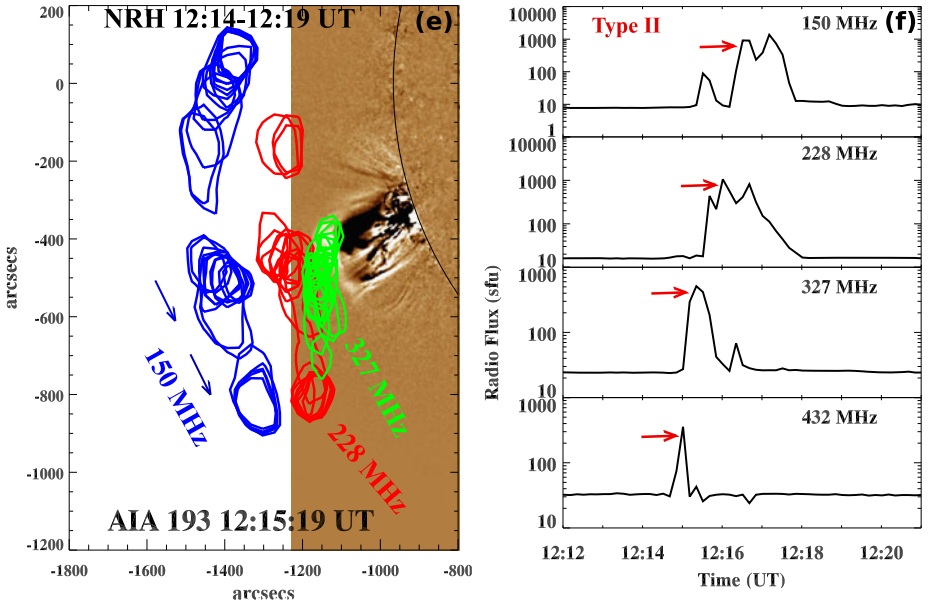

Figure 4 (*Continued.*)

line the time of break-out, as deduced from the change in structure of the plasmoid leading edge, shown in the bottom row of Figure 5.

The images at 171 and 193 Å show the broad bright front of the EUV waves generated at onset, followed by dimming north and south of the flux rope (Figure 5a). Loop brightening and oscillations appeared immediately behind the front across most of the central region. The early wave fronts are not visible in images of the hotter, 131 Å emission. The 131 Å image in the top row shows the expansion and contraction of the flux rope cavity, especially in the north, where the cavity edge lies along the inner edge of the 193 Å faint front indicated with an arrow in Figure 5b. At the time of the second dashed line the cavity expansion changed to contraction.

As mentioned above, the second dashed line in Figure 5 was placed to coincide with the time that the plasmoid changed shape. The leading front in the 193 and 131 Å space–time images in the bottom row split at the time of the second dashed line: the plasmoid slowed down while the fast front seen in 193 Å images continued through the corona. At this time, the 193 Å loop opened up and the bright 131 Å flux rope changed from circular to concave (Cheng *et al.*, 2011; Zimovets *et al.*, 2012), and apparently there was a fundamental change in the plasmoid propagation. We associate this sudden change with break-out. We also note that according to Figure 5f, the current sheet formed about 30 s (two frames) before the second dashed line. Thus the current sheet formed while the cavity was still expanding.

The structural changes are best seen in the accompanying movies, which are two-color composites of the 131 and 94 Å, and the 131 and 171 Å emissions. A few frames from the movies are shown in Figure 6. The top two rows show the emission at onset and the last row shows the hot post-eruption loops as seen in the 131/94 Å images. The selected images show that initially (around 12:13:24 UT), a bright tongue of 94 Å emission appeared above the 131 Å flare emission and 171 Å waves. The tongue then separated and was filled with the plasmoid or flux rope of hotter 131 Å emission. In the image shown in Figure 6d, the 131 Å plasmoid appears to be encased in a cocoon of 94 and 131 Å emission. At the northern edge

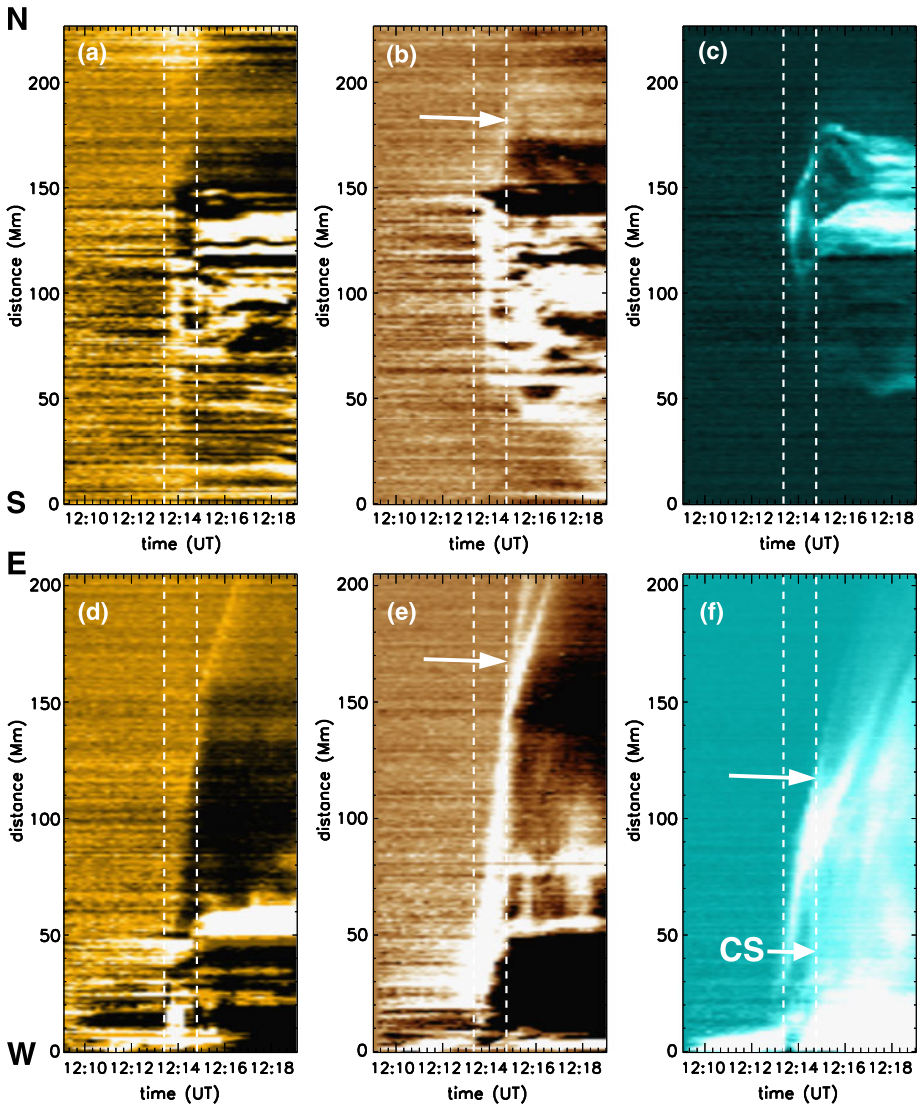

Figure 5 Time-distance images along lines shown in Figure 6b. (a) 171 Å along the S–N line; (b) 193 Å along the S–N line; (c) 131 Å along the S–N line; (d) 171 Å along the W–E line; (e) 193 Å along the W–E line; (f) 131 Å along the W–E line. The first dashed line indicates the flare onset and the second break-out time. The arrows point to fronts mentioned in the text.

of the cocoon close to the limb, bright 94 Å emission appeared. This seems to have been early low-lying loops in the bright flare arcade seen in Figure 6f. In the south of the plasmoid cavity, a region of faint, hot emission is just visible. The 131 Å image at 12:14:45 UT was also shown in White, Verwichte, and Foullon (2012), who commented on the faint line of hot emission, indicated by an arrow, which runs from the plasmoid to the site of the hot loop seen later in 131 Å images, and is shown in Figure 6f. The 94 Å emission, especially the

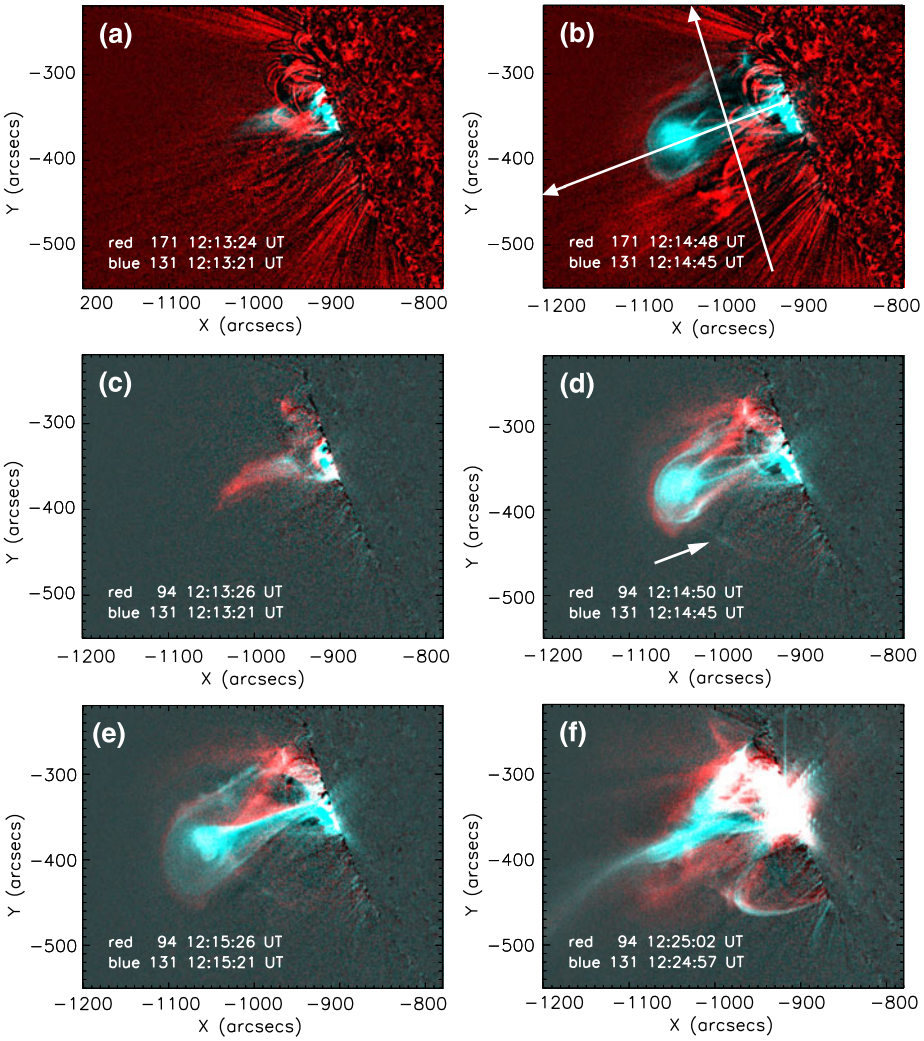

Figure 6 Evolution of hot plasma in the context of oscillating loops seen in 171 Å channel. (a and b) 171 Å and 131 Å composites; (c – f) 94 Å and 131 Å composites. In panel (b) the white lines show the position of the time–distance images in Figure 5. The top row shows frames from the movie *131_171.avi* and the other four frames are taken from the movie *131_94.avi*.

emission seen at 12:25:02 UT, suggests that this line of 131 Å emission outlined the top of a hot-loop arcade that formed at the time of break-out.

2.4. STEREO View of the Flare Site

This flare, which was seen over the east limb from Earth, was observed near disk center in the STEREO-B/EUVI (hereafter EUVI-B) images. Savage *et al.* (2012) have identified the main flare footpoints and flaring loops in the EUVI-B 195 Å images. At 195 Å, the cool plumes and loops are less visible than at 171 Å. Therefore, in Figure 7, we show the 171 Å EUVI-B and AIA images. Unfortunately, the EUVI-B image is partially saturated by the

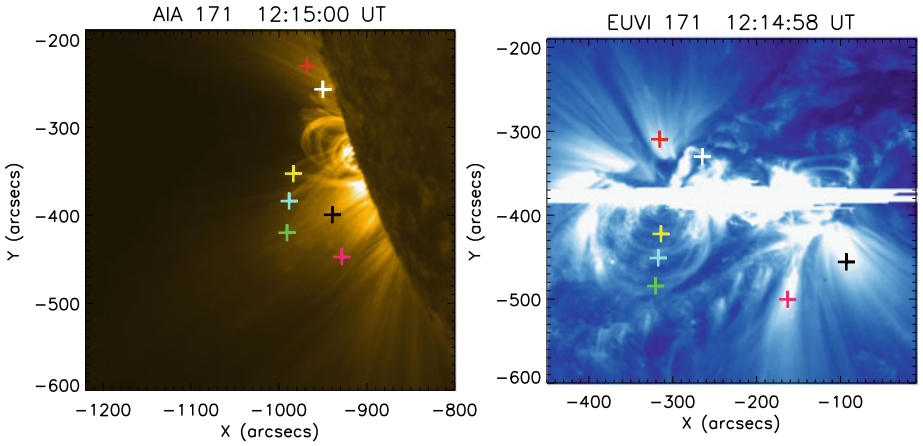

Figure 7 Co-temporal images of AIA 171 and STEREO-B 171 Å for identifying loops and plumes. Crosses of the same color identify the same points in the two images.

flare emission, so that loops that were below and along the line-of-site to the erupting flux rope are not visible. However, the loops that were located to the north and south and the sites of the plumes are clearly visible.

To find the positions of structures from the different perspectives, we used the SolarSoft routine scc_measure.pro (Thompson, 2006). We selected a point on the AIA image and then identified the same feature on the epipolar line drawn on the EUVI-B image. The same positions are marked with the same color cross in the two images. The EUVI image shows that the plumes were more than 100 arcsecs away from the flare site. We note that there was an arcade of large loops to the south and a faint (in 171 Å) arcade of loops to the north linking the flare footpoints, as identified in Savage *et al.* (2012).

3. Summary and Discussion

We have taken a second look at the waves and structures observed by SDO/AIA during a flare eruption that occurred on 3 November 2010 on the east limb of the Sun as seen from Earth. At flare onset, fast 1000 – 2000 km s^{-1} EUV waves were seen propagating along cool (1 MK) plume-like structures that were situated about 100 arcsec from the flare site, and were headed by decimetric emission. These waves were traveling ahead and alongside a fast, flare-heated plasmoid seen in 131 Å images. Loops ahead of the plasmoid, heated to about 5 MK, were seen in the 94 Å channel images. Figure 8a is a simplified sketch of the various features.

When the hot plasmoid reached the apex of the pre-flare loops, the leading edge of the plasmoid accelerated away from the main core. At the same time, hot loops were seen below and to the side of the plasmoid, and the region below collapsed inward to fill the space evacuated by the outward-moving plasmoid, as sketched in Figure 8b.

Initially, flaring in the low corona/chromosphere caused a rapid pressure increase, flux rope destabilization, cavity expansion, and high-energy particles. Waves propagated outward in all directions. Heating was confined to the inner flux-rope structure and its cavity. The rapidly rising flux rope soon encountered the overlying arcade. Reconnection with the overlying field led to break-out (Antiochos, DeVore, and Klimchuk, 1999;

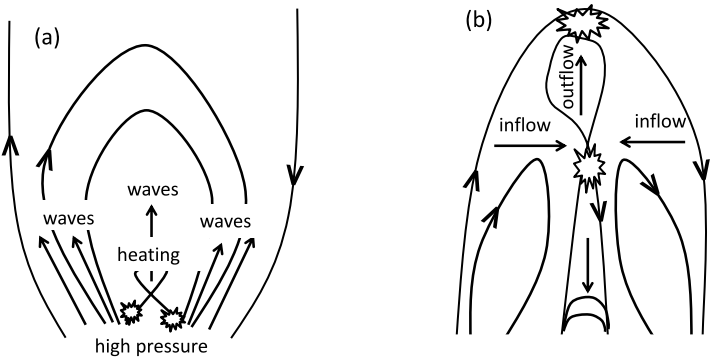

Figure 8 Sketch of the loop system at the time of the (a) flare onset and (b) break-out. Reconnection sites are shown as explosions.

Karpen, Antiochos, and DeVore, 2012). The formation of high-lying, hot loops alongside and just below the plasmoid and the plasma inflows were a consequence of break-out. Post-flare loops appeared below the plasmoid, close to the limb. Since the eruption occurred over the limb as seen from Earth, it is not possible to determine the exact flare site, the magnetic field configuration, or the flare trigger. However, the STEREO 171 Å image (right panel of Figure 7) shows the complex quadrupolar magnetic field configuration associated with a possible null point above the flare site, which are needed for the breakout reconnection.

This scenario is very different from previous ones for this event in two respects. First, we discovered fast waves at the onset of the flare, which led to the interpretation that a blast wave and not a piston-driven shock caused the type-II radio emission. Second, we noted that the inflows occurred when the plasmoid structure changed and the overlying 193 Å loop structure opened up, and thus concluded that the inflows are a consequence of the break-out. In this scenario, the bright 131 Å thread that was below the plasmoid could be either the current sheet or a newly-formed loop seen edge on. The observation of hard X-ray emission near the plasmoid (Bain *et al.*, 2012) favor the current-sheet interpretation, but the width of the emission and its stability suggest that it may be a newly formed loop similar to those seen on either side of the plasmoid.

We were unable to observe the formation of a piston-driven shock in the AIA 211 and 193 Å running difference images as observed in other flux-rope eruption events (Ma *et al.*, 2011; Kozarev *et al.*, 2011; Gopalswamy *et al.*, 2012). The flux rope is heavily decelerated (mean speed ≈ 241 km s^{-1}) in the interplanetary (IP) medium, and there was no piston-driven shock in the IP space (*e.g.*, IP type-II radio burst). Moreover, there is no strong lateral expansion of the flux rope that could be sufficient to drive the shock at the flanks of the CME (Patsourakos and Vourlidas, 2012). We observed fast waves simultaneously at both sides of the flux-rope (along the plumes), therefore it is also possible that the pressure pulse over-ran the flux rope, causing acceleration of the plasmoid in the low corona. Flare-heated plasma was observed at the flare site, in the flux-rope, and along loops outlining the surrounding cavity, suggesting significant heating throughout the flux rope cavity, not just along the central current sheet (see movie *131_94.avi*).

In conclusion, we reported a unique multiwavelength observation of the fast propagating EUV waves in AIA 171 Å and associated radio emissions ahead of these waves, which supports the flare blast-wave scenario as a possible candidate to generate high-frequency type-II radio bursts. However, a more in-depth analysis of such events will be helpful for understanding the eruption processes associated with the generation of these fast waves.

Acknowledgements We would like to thank the referee for his/her constructive comments and suggestions, which improved the manuscript considerably. SDO is a mission for NASA's Living With a Star (LWS) Program. We are thankful for the radio data obtained from NRH. PK is highly thankful to P.K. Manoharan for the helpful discussions on radio observations. This work is supported by the "Development of Korea Space Weather Center" project, and the KASI basic research fund.

References

Antiochos, S.K., DeVore, C.R., Klimchuk, J.A.: 1999, A model for solar coronal mass ejections. *Astrophys. J.* **510**, 485 – 493. doi:10.1086/306563.

Bain, H.M., Krucker, S., Glesener, L., Lin, R.P.: 2012, Radio imaging of shock-accelerated electrons associated with an erupting plasmoid on 2010 November 3. *Astrophys. J.* **750**, 44. doi:10.1088/0004-637X/750/1/44.

Carmichael, H.: 1964, A process for flares. In: Hess, W.N. (ed.) *The Physics of Solar Flares, NASA SP-50*, 451 – 456.

Cheng, X., Zhang, J., Liu, Y., Ding, M.D.: 2011, Observing flux rope formation during the impulsive phase of a solar eruption. *Astrophys. J. Lett.* **732**, L25. doi:10.1088/2041-8205/732/2/L25.

Foullon, C., Verwichte, E., Nakariakov, V.M., Nykyri, K., Farrugia, C.J.: 2011, Magnetic Kelvin–Helmholtz instability at the Sun. *Astrophys. J. Lett.* **729**, L8. doi:10.1088/2041-8205/729/1/L8.

Gopalswamy, N., Nitta, N., Akiyama, S., Mäkelä, P., Yashiro, S.: 2012, Coronal magnetic field measurement from EUV images made by the Solar Dynamics Observatory. *Astrophys. J.* **744**, 72. doi:10.1088/0004-637X/744/1/72.

Hannah, I.G., Kontar, E.P.: 2012, Multi-thermal dynamics and energetics of a coronal mass ejection in the low solar atmosphere. arXiv:1212.5529.

Hirayama, T.: 1985, Modern observations of solar prominences. *Solar Phys.* **100**, 415 – 434. doi:10.1007/BF00158439.

Howard, R.A., Moses, J.D., Vourlidas, A., Newmark, J.S., Socker, D.G., Plunkett, S.P., Korendyke, C.M., Cook, J.W., Hurley, A., Davila, J.M., Thompson, W.T., St Cyr, O.C., Mentzell, E., Mehalick, K., Lemen, J.R., Wuelser, J.P., Duncan, D.W., Tarbell, T.D., Wolfson, C.J., Moore, A., Harrison, R.A., Waltham, N.R., Lang, J., Davis, C.J., Eyles, C.J., Mapson-Menard, H., Simnett, G.M., Halain, J.P., Defise, J.M., Mazy, E., Rochus, P., Mercier, R., Ravet, M.F., Delmotte, F., Auchere, F., Delaboudiniere, J.P., Bothmer, V., Deutsch, W., Wang, D., Rich, N., Cooper, S., Stephens, V., Maahs, G., Baugh, R., McMullin, D., Carter, T.: 2008, Sun Earth Connection Coronal and Heliospheric Investigation (SECCHI). *Space Sci. Rev.* **136**, 67 – 115. doi:10.1007/s11214-008-9341-4.

Innes, D.E., Curdt, W., Schwenn, R., Solanki, S., Stenborg, G., McKenzie, D.E.: 2001, Large Doppler shifts in X-ray plasma: An explosive start to coronal mass ejection. *Astrophys. J. Lett.* **549**, L249 – L252. doi:10.1086/319164.

Karpen, J.T., Antiochos, S.K., DeVore, C.R.: 2012, The mechanisms for the onset and explosive eruption of coronal mass ejections and eruptive flares. *Astrophys. J.* **760**, 81. doi:10.1088/0004-637X/760/1/81.

Kerdraon, A., Delouis, J.M.: 1997, The Nançay Radioheliograph. In: Trottet, G. (ed.) *Coronal Physics from Radio and Space Observations*, *Lecture Notes in Physics* **483**, Springer, Berlin, 192 – 201. doi:10.1007/BFb0106458.

Kopp, R.A., Pneuman, G.W.: 1976, Magnetic reconnection in the corona and the loop prominence phenomenon. *Solar Phys.* **50**, 85 – 98. doi:10.1007/BF00206193.

Kozarev, K.A., Korreck, K.E., Lobzin, V.V., Weber, M.A., Schwadron, N.A.: 2011, Off-limb solar coronal wavefronts from SDO/AIA Extreme-ultraviolet Observations: Implications for particle production. *Astrophys. J. Lett.* **733**, L25. doi:10.1088/2041-8205/733/2/L25.

Lemen, J.R., Title, A.M., Akin, D.J., Boerner, P.F., Chou, C., Drake, J.F., Duncan, D.W., Edwards, C.G., Friedlaender, F.M., Heyman, G.F., Hurlburt, N.E., Katz, N.L., Kushner, G.D., Levay, M., Lindgren, R.W., Mathur, D.P., McFeaters, E.L., Mitchell, S., Rehse, R.A., Schrijver, C.J., Springer, L.A., Stern, R.A., Tarbell, T.D., Wuelser, J.P., Wolfson, C.J., Yanari, C., Bookbinder, J.A., Cheimets, P.N., Caldwell, D., Deluca, E.E., Gates, R., Golub, L., Park, S., Podgorski, W.A., Bush, R.I., Scherrer, P.H., Gummin, M.A., Smith, P., Auker, G., Jerram, P., Pool, P., Soufli, R., Windt, D.L., Beardsley, S., Clapp, M., Lang, J., Waltham, N.: 2012, The Atmospheric Imaging Assembly (AIA) on the Solar Dynamics Observatory (SDO). *Solar Phys.* **275**, 17 – 40. doi:10.1007/s11207-011-9776-8.

Lin, R.P., Dennis, B.R., Hurford, G.J., Smith, D.M., Zehnder, A., Harvey, P.R., Curtis, D.W., Pankow, D., Turin, P., Bester, M., Csillaghy, A., Lewis, M., Madden, N., van Beek, H.F., Appleby, M., Raudorf, T., McTiernan, J., Ramaty, R., Schmahl, E., Schwartz, R., Krucker, S., Abiad, R., Quinn, T., Berg, P.,

Hashii, M., Sterling, R., Jackson, R., Pratt, R., Campbell, R.D., Malone, D., Landis, D., Barrington-Leigh, C.P., Slassi-Sennou, S., Cork, C., Clark, D., Amato, D., Orwig, L., Boyle, R., Banks, I.S., Shirey, K., Tolbert, A.K., Zarro, D., Snow, F., Thomsen, K., Henneck, R., McHedlishvili, A., Ming, P., Fivian, M., Jordan, J., Wanner, R., Crubb, J., Preble, J., Matranga, M., Benz, A., Hudson, H., Canfield, R.C., Holman, G.D., Crannell, C., Kosugi, T., Emslie, A.G., Vilmer, N., Brown, J.C., Johns-Krull, C., Aschwanden, M., Metcalf, T., Conway, A.: 2002, The Reuven Ramaty High-Energy Solar Spectroscopic Imager (RHESSI). *Solar Phys.* **210**, 3 – 32. doi:10.1023/A:1022428818870.

Ma, S., Raymond, J.C., Golub, L., Lin, J., Chen, H., Grigis, P., Testa, P., Long, D.: 2011, Observations and interpretation of a low coronal shock wave observed in the EUV by the SDO/AIA. *Astrophys. J.* **738**, 160. doi:10.1088/0004-637X/738/2/160.

Magdalenić, J., Vršnak, B., Pohjolainen, S., Temmer, M., Aurass, H., Lehtinen, N.J.: 2008, A flare-generated shock during a coronal mass ejection on 24 December 1996. *Solar Phys.* **253**, 305 – 317. doi:10.1007/s11207-008-9220-x.

Magdalenić, J., Marqué, C., Zhukov, A.N., Vršnak, B., Žic, T.: 2010, Origin of coronal shock waves associated with slow coronal mass ejections. *Astrophys. J.* **718**, 266 – 278. doi:10.1088/0004-637X/718/1/266.

Magdalenić, J., Marqué, C., Zhukov, A.N., Vršnak, B., Veronig, A.: 2012, Flare-generated type II burst without associated coronal mass ejection. *Astrophys. J.* **746**, 152. doi:10.1088/0004-637X/746/2/152.

Patsourakos, S., Vourlidas, A.: 2012, On the nature and genesis of EUV waves: A synthesis of observations from SOHO, STEREO, SDO, and Hinode (Invited review). *Solar Phys.* **281**, 187 – 222. doi:10.1007/s11207-012-9988-6.

Pesnell, W.D., Thompson, B.J., Chamberlin, P.C.: 2012, The Solar Dynamics Observatory (SDO). *Solar Phys.* **275**, 3 – 15. doi:10.1007/s11207-011-9841-3.

Reeves, K.K., Golub, L.: 2011, Atmospheric Imaging Assembly observations of hot flare plasma. *Astrophys. J. Lett.* **727**, L52. doi:10.1088/2041-8205/727/2/L52.

Savage, S.L., Holman, G., Reeves, K.K., Seaton, D.B., McKenzie, D.E., Su, Y.: 2012, Low-altitude reconnection inflow-outflow observations during a 2010 November 3 solar eruption. *Astrophys. J.* **754**, 13. doi:10.1088/0004-637X/754/1/13.

Sturrock, P.A.: 1966, Model of the high-energy phase of solar flares. *Nature* **211**, 695 – 697. doi:10.1038/211695a0.

Thompson, W.T.: 2006, Coordinate systems for solar image data. *Astron. Astrophys.* **449**, 791 – 803. doi:10.1051/0004-6361:20054262.

Tothova, D., Innes, D.E., Stenborg, G.: 2011, Oscillations in the wake of a flare blast wave. *Astron. Astrophys.* **528**, L12. doi:10.1051/0004-6361/201015272.

Vršnak, B., Cliver, E.W.: 2008, Origin of coronal shock waves. Invited review. *Solar Phys.* **253**, 215 – 235. doi:10.1007/s11207-008-9241-5.

Vršnak, B., Lulić, S.: 2000a, Formation of coronal MHD shock waves – I. The basic mechanism. *Solar Phys.* **196**, 157 – 180. doi:10.1023/A:100523680472.

Vršnak, B., Lulić, S.: 2000b, Formation of coronal MHD shock waves – II. The pressure pulse mechanism. *Solar Phys.* **196**, 181 – 197. doi:10.1023/A:1005288310697.

Vršnak, B., Warmuth, A., Temmer, M., Veronig, A., Magdalenić, J., Hillaris, A., Karlický, M.: 2006, Multi-wavelength study of coronal waves associated with the CME-flare event of 3 November 2003. *Astron. Astrophys.* **448**, 739 – 752. doi:10.1051/0004-6361:20053740.

White, R.S., Verwichte, E.: 2012, Transverse coronal loop oscillations seen in unprecedented detail by AIA/SDO. *Astron. Astrophys.* **537**, A49. doi:10.1051/0004-6361/201118093.

White, R.S., Verwichte, E., Foullon, C.: 2012, First observation of a transverse vertical oscillation during the formation of a hot post-flare loop. *Astron. Astrophys.* **545**, A129. doi:10.1051/0004-6361/201219856.

Zimovets, I., Vilmer, N., Chian, A.C.L., Sharykin, I., Struminsky, A.: 2012, Spatially resolved observations of a split-band coronal type II radio burst. *Astron. Astrophys.* **547**, A6. doi:10.1051/0004-6361/201219454.